Long-chain plant wax *n*-alkane hydrogen isotopic evidence for increased Little Ice Age aridity in the midcontinental United States.

[*,1,2] Broxton W. Bird, [3,4]Erika J. Freimuth, and [3]Aaron F. Diefendorf

[1]Department of Earth and Environmental Sciences, Indiana University, Indianapolis, IN, 46202, USA.
[2]Center for Earth and Environmental Science, Indiana University, Indianapolis, IN, 46202, USA.
[3]Department of Geosciences, University of Cincinnati, Cincinnati, OH, 45221, USA.
[4]Climate Central, Princeton, New Jersey, 08542, USA.

*Corresponding Author: bwbird@iu.edu

Key Words
Hydroclimate, Paleoclimate, Common Era, Medieval Climate Anomaly, Current Warm Period

Abstract

We compare hydrogen isotopic measurements of long-chain leaf-wax *n*-alkanes (δ^2H_w; C_{27}, C_{29}, and C_{31}) from Martin Lake, IN, United States of America (USA), with a calcite-based reconstruction of the oxygen isotopic composition of precipitation ($\delta^{18}O_p$) from the same lake. We observe stable and high δ^2H_w during the Common Era (last 2000 years), which we interpret as growing-season precipitation originating mainly from the Gulf of Mexico and Atlantic. During the Little Ice Age (LIA; 1200-1850 CE), δ^2H_w values increased by 3-8 ‰, concomitant with a significant decrease in $\delta^{18}O_p$ values by up to 12.5 ‰. Multiple proxy records for this time indicate persistent growing-season drought. We interpret these relatively high δ^2H_w values, as compared to the $\delta^{18}O_p$ values, as a signal of low relative humidity that resulted in an ^2H enrichment in plant source water resulting in high δ^2H values through enhanced plant water and/or soil evaporation. These results support the occurrence of low humidity conditions during the LIA in the midcontinental USA that also contributed to the marked decline of regional pre-Columbian Mississippian populations.

Introduction

The hydrogen isotopic composition of long-chain plant wax *n*-alkanes (δ^2H_w) reflects the δ^2H of biosynthetically available source water (δ^2H_{sw}) used by terrestrial plants during photosynthesis (Kahmen et al., 2013b; Smith and Freeman, 2006). Modern calibration studies have linked δ^2H_{sw} and δ^2H_w to the hydrogen isotopic composition of precipitation (δ^2H_p) (Garcin et al., 2012; Rao et al., 2009; Sachse et al., 2004), supporting the use of δ^2H_w as a paleohydrological proxy for annual average δ^2H_p. Though more commonly used in tropical regions (e.g., Bird et al., 2014; Sachse et al., 2012; Thomas et al., 2014; Tierney et al., 2008), an increasing number of δ^2H_w records are being developed in midlatitude temperate regions (e.g., Muñoz et al., 2020; Puleo et al., 2020; Schartman et al., 2020). Unlike monsoon regions that experience pronounced wet and dry seasons, midlatitude regions, like the midcontinental United States of America (USA), can receive precipitation throughout the year, the isotopic composition of which changes seasonally depending on the source from which it was derived (Bird et al., 2017; Liu et al., 2014). Remarkably little variability has been observed in new compound specific δ^2H records from the midcontinental USA (Muñoz et al., 2020; Puleo et al., 2020), which has been suggested to reflect long-term stability in annual average δ^2H_p. This stands in contrast to reconstructions of the oxygen isotopic composition of precipitation ($\delta^{18}O_p$) based on authigenic calcite ($\delta^{18}O_c$), which demonstrate large amplitude variability during the Medieval Climate Anomaly (MCA; 950-1250 CE), Little Ice Age (LIA; 1250-1850 CE) and current warm period (CWP; last ca. 100 years) (Bird et al., 2017).

Here, we evaluate the hydroclimatic significance of a new long-chain plant wax *n*-alkane δ^2H_w record from Martin Lake, Indiana (IN), in the context of a previously published $\delta^{18}O_c$-based $\delta^{18}O_p$ reconstruction spanning the last 2000 years from the same lake (Bird et al., 2017). Martin Lake was specifically selected to evaluate δ^2H_w as a proxy for δ^2H_p in the midcontinental USA because it is hydrologically open with a relatively small watershed and has a well-constrained $\delta^{18}O_c$ reconstruction of $\delta^{18}O_p$ (Bird et al., 2017). Other hydroclimate proxies measured at the lake provide additional information about regional temperature trends (carbon isotopic composition of calcite; $\delta^{13}C_c$) and the occurrence of warm-season rainstorm events (%lithics) during the last 2000 years. With these data, we investigate δ^2H_w and $\delta^{18}O_c$ variability during the MCA, LIA and CWP and test the hypothesis that δ^2H_w reliably captures changes in annual average δ^2H_p. If true, δ^2H_w should broadly track $\delta^{18}O_p$ at Martin Lake. If otherwise, additional factors and alternative interpretations of δ^2H_w may need to be considered.

Study Area and Background

Martin Lake is a small monomictic kettle in LaGrange County, IN (41.56°, -85.38°, 274 m ASL; Fig. 1). Its bathymetry is steep sided and flat bottomed, with a maximum depth of 17 m. Martin Lake's watershed is small (12.86 km^2) and relatively flat, with an elevation range of 125 m. Vegetation is primarily deciduous eastern hardwood forest that was stable during the last 2000 years until Euro-American land clearance began in the 1800s (Williams, 1974). Regional precipitation averages ca. 910 mm yr^{-1}, which equates to 1.18×10^7 m^3 over the watershed. This is more than 10 times Martin Lake's volume (1.11×10^6 m^3) and results in a ca. 3-month residence time (New, 2009). Hydrologically open conditions are reflected in lake water δ^2H (δ^2H_L) and $\delta^{18}O$ ($\delta^{18}O_L$) measurements, which plot on the regional meteoric water line (RMWL) at the intersection with the regional evaporation line (REL), indicating that they are not impacted by evaporation and instead reflect the annual average δ^2H_p and $\delta^{18}O_p$ (Fig. 1C, D). The $\delta^{18}O$ values of modern authigenic calcite ($\delta^{18}O_c$) match those predicted for $\delta^{18}O_L$ (Kim and O'Neil, 1997), demonstrating that $\delta^{18}O_c$ is precipitated in equilibrium with $\delta^{18}O_L$ and that they reflect annual average $\delta^{18}O_p$ (Bird et al., 2017).

Like much of the Midwest, climate and $\delta^{18}O_p$ and δ^2H_p vary seasonally at Martin Lake. Enhanced clockwise atmospheric circulation over the Gulf of Mexico and midcontinental USA during the warm season (April – November) draws ^{18}O and ^2H enriched moisture (-5.5 ‰ & -33.8 ‰, respectively) from the Gulf of Mexico and Atlantic into the region that is precipitated by west to east moving frontal convective systems (Andresen et al., 2012; Bird et al., 2017). Enhanced ridge and trough atmospheric circulation during the cold season (December – March) typically delivers ^{18}O and ^2H depleted moisture (-16.4 ‰ & -126.2 ‰, respectively) from the Pacific and/or Arctic (Bird et al., 2017). Changes in the frequency of precipitation events from these primary moisture sources is directly related to the Pacific North American teleconnection (PNA), which has strong and significant correlations with precipitation and isotope variability in the midcontinental USA (Coleman and Rogers, 2003; Leathers et al., 1991; Liu et al., 2014). In general, negative (-) PNA conditions resemble warm-season circulation, precipitation, and isotope patterns while positive (+) PNA conditions resemble cold-season patterns.

Changes in atmospheric circulation resembling negative and positive PNA mean states have long been suggested to have occurred in the midcontinental USA during the Holocene. Based initially on pollen data (Webb, 1985), an increasing number of multi-proxy and isotope-based studies support this assertion (Baker et al., 1998; Bird et al., 2017; Booth et al., 2006; Wright et al., 2023). At Martin Lake, $\delta^{18}O_c$, $\delta^{13}C_c$, and lithic abundances (%lithics) indicate that significant changes in atmospheric circulation resembling PNA-like mean states influenced the source and seasonality of precipitation in the midcontinental USA during MCA, LIA, and CWP (Bird et al., 2017). During the MCA and CWP, these proxies indicate more frequent warm-season rain events (+%lithics) from the Gulf of Mexico and Atlantic (+$\delta^{18}O_c$) when regional temperatures were warm (+$\delta^{13}C_c$; -PNA-like). During the LIA, the proxy data indicate cool (-$\delta^{13}C_c$), dry warm-seasons (-%lithics), and longer, snowier winters with moisture derived from the Pacific and Arctic (-$\delta^{18}O_c$), consistent with +PNA-like conditions. The consistency of these data with other regional paleoclimate records (e.g., Bird et al., 2019; Booth et al., 2006; Gibson et al., 2022; Laird et al., 1998; Pompeani et al., 2021; Wright et al., 2023) supports the widespread occurrence of rapid hydroclimate changes (e.g., severe LIA drought) during the MCA and LIA.

Methodology

Twenty-nine sediment samples were selected from the top ca. 2 m of the Martin Lake composite core at 8- to10-cm intervals for biomarker analysis at the University of Cincinnati. All samples were freeze-dried and homogenized. Lipid extraction followed the methods reported in Freimuth et al. (2020). Briefly, lipids were extracted from 0.5-2.5 g of sediment using an Accelerated Solvent Extractor (ASE 350, Dionex) with dichloromethane/methanol (5:1, v v^{-1}). Lipid extracts were base saponified and then separated into neutral and acid fractions over aminopropyl-bonded silica gel. The neutral fraction was further separated into aliphatic and polar fractions over alumina oxide and the aliphatic fraction was further separated over 5 % silver nitrate silica gel to isolate the saturated hydrocarbons that include the *n*-alkanes. *n*-Alkanes were identified and quantified using an Agilent gas chromatograph (GC) mass spectrometer (MS) and flame ionization detector (GC-FID) using *n*-alkane standards.

Compound-specific hydrogen isotopes of *n*-C_{27}, *n*-C_{29}, and *n*-C_{31} alkanes were measured using a Thermo Electron Delta V Advantage isotope ratio MS connected to a Thermo Trace GC

Ultra coupled to an Isolink pyrolysis reactor. Data were normalized to the VSMOW/SLAP scale using a standard *n*-alkane mix of known δ^2H composition (Mix A5; A. Schimmelmann, Indiana University). The long-term analytical precision was measured following Polissar and D'Andrea (2013) and is 3.3 ‰ (n = 187).

The composition of odd-chain *n*-alkanes is commonly compared among plants using the average chain length (ACL) metric following Diefendorf and Freimuth (2017) where:

$$ACL = (25n\text{-}C_{25} + 27n\text{-}C_{27} + 29n\text{-}C_{29} + 31n\text{-}C_{31} + 33n\text{-}C_{33} + 35n\text{-}C_{35}) / (n\text{-}C_{25} + n\text{-}C_{27} + n\text{-}C_{29} + n\text{-}C_{31} + n\text{-}C_{33} + n\text{-}C_{35})$$

To characterize differences in odd chain length preference, the carbon preference index (CPI) was measured using the Marzi et al. (1993) equation where:

$$CPI = (n\text{-}C_{23} + n\text{-}C_{25} + n\text{-}C_{27} + n\text{-}C_{29} + n\text{-}C_{31}) + (n\text{-}C_{25} + n\text{-}C_{27} + n\text{-}C_{29} + n\text{-}C_{31} + n\text{-}C_{33}) / (2(n\text{-}C_{24} + n\text{-}C_{26} + n\text{-}C_{28} + n\text{-}C_{30} + n\text{-}C_{32}))$$

P_{aq}, a proxy for quantifying submerged or floating aquatic plant material vs. emergent and terrestrial material, based on *n*-alkanes, was measured using the equation in Ficken et al. (2000) where:

$$P_{aq} = (n\text{-}C_{23} + n\text{-}C_{25}) / (n\text{-}C_{23} + n\text{-}C_{25} + n\text{-}C_{29} + n\text{-}C_{31})$$

Methods for δ^{18}O, δ^{13}C, %lithics and radiometric dating at Martin Lake are described in (Bird et al., 2017).

Results

Concentration data for all *n*-alkane chain lengths were generally low and stable except for a prominent peak centered at 1500 CE (Fig. 2). The average chain length (ACL) for the record ranged between 29.8 and 28.4 (average = 29.1), with a carbon preference index (CPI) averaging 10.2, except for a peak of 32.6 at ca. 1370 CE, and a Paq index between 0.120-0.303 (average = 0.186) (Fig. 2) (Ficken et al., 2000; Marzi et al., 1993). δ^2H_w values for *n*-alkane C_{27}, C_{29}, and

C_{31} decreased during the last 2000 years with *n*-C_{31} showing the steepest negative slope (m = -5.068 x 10^{-3}) (Fig. 3). Considerable high-frequency variability was superimposed on the long-term trends, with *n*-C_{27}, *n*-C_{29}, and *n*-C_{31} δ^2H_w values respectively varying by 27.7, 23.3, and 26.7 ‰ (Fig. 3). Relative to their long-term trends, δ^2H_w values for all chain lengths showed generally low to average values between 0 and ca. 1110 CE, with *n*-C_{27} showing a one-sample peak at ca. 750 CE and *n*-C_{29} and *n*-C_{31} showing a broader increase from ca. 550 to 800 CE. Between 1200 and 1840 CE, δ^2H_w values and variability increased across all chain lengths with peaks between 1200-1300, 1380-1600, and 1700-1850 CE. After 1850 CE, δ^2H_w values for all chain lengths decreased.

Discussion

In contrast to the hypothesized in-phase relationship between δ^2H_w and $\delta^{18}O_c$, the long-term $\delta^{18}O_c$ trend was positive over the last 2000 years (Fig. 4B). Higher frequency variability was also anti-phased, with low δ^2H_w during the MCA and CWP when $\delta^{18}O_c$ was high, and vice versa for the LIA (Fig. 4A & B; Table 1). Given the relationships between average annual $\delta^{18}O_p$, $\delta^{18}O_L$, and $\delta^{18}O_c$, at Martin Lake, $\delta^{18}O_c$ and δ^2H_w anti-phasing indicates that δ^2H_{sw} did not reflect annual average δ^2H_p at Martin Lake during at least the last 2000 years. Because plant waxes are synthesized during the growing season (Freimuth et al., 2017; Tipple et al., 2013), it is likely that δ^2H_{sw}, and hence δ^2H_w, instead reflected growing-season δ^2H_p (e.g., Schartman et al., 2020), possibly reflecting subsurface groundwater compartmentalization (e.g., Evaristo et al., 2015).

This is consistent with the relatively narrow 30 ‰ range in δ^2H compared to the range observed in modern δ^2H_p and predicted for past δ^2H_w variability based on $\delta^{18}O_c$ (both ca. 90 ‰; Table 1). Converting δ^2H_w to δ^2H_p using an epsilon factor of 107 ‰ (Freimuth et al., 2017) places reconstructed δ^2H_p between ca. -80 and -50 ‰ with a long-term average of -63 ‰ for all chain lengths (Fig. 4A; Table 1). These values are consistent with warm-season precipitation derived from the Gulf of Mexico and Atlantic (ca. -43 ‰) and modern annual average δ^2H_p (ca. -60 ‰), which is predominated by warm-season precipitation (75 %) relative to cold-season precipitation (25 %), but are far higher than cold-season precipitation derived from the Pacific and Arctic (ca. -125 ‰) (Bird et al., 2017).

If δ^2H_w captures warm-season precipitation, what are the hydroclimatic implications of increased δ^2H_w during cooler and drier periods (e.g., the LIA) and decreased δ^2H_w during warmer and wetter periods (e.g., the MCA and CWP)? One possibility is that δ^2H_w could reflect rainout from air masses originating in the Gulf of Mexico and Atlantic (i.e., the amount effect) (Gat, 1996). Increased δ^2H_w during the LIA, for example, is consistent with evidence for less frequent warm-season precipitation events (low $\delta^{18}O_c$ and %lithics) and regional aridity. Soil and/or plant water evaporation could also have affected δ^2H_w (Kahmen et al., 2013a; Kahmen et al., 2013b; Smith and Freeman, 2006). Relative humidity, for instance, affects both soil and plant water evaporation, with reductions in growing-season humidity of 20 % increasing δ^2H_w by 11 ‰ in grasses (Smith and Freeman, 2006) with isotopic enrichments also noted for leaf waxes from deciduous trees (Feakins and Sessions, 2010; Kahmen et al., 2013b; Sachse et al., 2012). Similar humidity reductions are not unrealistic at Martin Lake and regionally during the LIA, possibly contributing to the 3 to 13 ‰ differences in δ^2H between the MCA, LIA, and CWP (Table 1; Bird et al., 2017; Booth et al., 2006; Pompeani et al., 2021).

Comparing the Martin and Horseshoe lake δ^2H_w records shows that both increased during the LIA by similar amounts (3-8 ‰ and 5 ‰, respectively; Fig. 4), suggesting regionally coherent hydroclimate processes. Increased evaporation during the LIA as a driver of δ^2H_w is consistent with significant evaporative enrichment of $\delta^{18}O_c$ at Horseshoe Lake (Pompeani et al., 2021), lower ground water tables in Michigan and Minnesota (Booth et al., 2006), reduced lithics at Martin Lake, and less frequent rainstorm-driven flooding on the White River, IN (Wright et al., 2023), which support regional increases evaporation and reductions in the amount of growing-season precipitation. The Martin and Horseshoe lake δ^2H_w records diverged during the CWP, however, with continued δ^2H_w increases at Horseshoe Lake while δ^2H_w declined at Martin Lake. This divergence could possibly reflect vegetation changes in response to Euro-American land clearance, including a dramatic increase in disturbance grasses (e.g., *Ambrosia*) since ca. 1850 CE (McAndrews, 1988; Munoz et al., 2015). A ca. 30 ‰ decrease in δ^2H_w is possible if all long-chain *n*-alkane leaf waxes were derived from C3 grasses like *Ambrosia* (Sachse et al., 2012), but nearby pollen data from Pretty Lake indicates the presence of forest cover even though *Ambrosia* pollen increased over the past 200 years (Williams, 1974). Nonetheless, while the decrease in δ^2H_w is consistent with a return to higher humidity during the last 200 years, it remains possible that the deep amplitude δ^2H_w low during the CWP may in part reflect an increase in disturbance grasses. At Horseshoe Lake, the increase in δ^2H_w during the CWP is more perplexing given the documented increase in *Ambrosia* at the site during the CWP (Munoz et al., 2014). One possibility is that local soil and/or pore water evaporation increased during the CWP, increasing δ^2H_w. It is also possible that recent trends reflect local or non-local hydrological signals given that an unknown fraction of plant waxes delivered to the lake may be derived from the upper Mississippi and/or Missouri river watersheds (Suh et al., 2019).

Conclusions

The isotopic range, and values of reconstructed δ^2H_p suggest that δ^2H_w reflects growing-season δ^2H_p, not annual average δ^2H_p. δ^2H_w stability indicates consistency in the source of growing season precipitation (i.e., the Gulf of Mexico and Atlantic) during the late Holocene. Increased δ^2H_w during the LIA likely reflects soil and/or plant water evaporation in response to reduced growing-season relative humidity (ca. –20 %) and precipitation, consistent with widespread regional evidence for low effective moisture in the midcontinental USA during this time. This illustrates that a multi-proxy approach is needed when interpreting midcontinental δ^2H_w records and that modern δ^2H_p calibrations under the current warm-season climate regime may not apply under cold-climate mean states (e.g., the Little Ice Age). Additional proxy calibration is needed if δ^2H_w is to be widely applied as a paleohydrological proxy in the midcontinental USA. If seasonally specific, δ^2H_w could yield important information about growing-season paleohydrological variability and its relationship with mean state atmospheric circulation changes reflected in records of the annual average isotopic composition of precipitation.

Data Availability

All original data is available on the NOAA Paleoclimatology Database:
https://www.ncei.noaa.gov/access/paleo-search/study/39005

Funding Declaration

This work was supported by awards EAR-1903628 and EAR-1636740 from the National Science Foundation.

Competing Interest Declaration

There were no competing interests.

Figure Captions

Figure 1 Composite mean maps of (A) cold-season (Dec-Mar) and (B) warm-season (Apr-Nov) 850 hPa vector winds between 1949-2015 from the NCEP-NCAR reanalysis database. Black arrows are wind directions with colored shading indicating velocity (m s^{-1}). Also plotted are mean back trajectories for cluster 1 (thick white line in A) and cluster 2 (thick red line in B) of the event-based Indianapolis, IN, precipitation samples. White squares are spaced at 24 hr intervals. White circles indicate the starting point from which back trajectories were calculated. The mean back trajectories are in good agreement with their respective seasonal atmospheric circulation patterns since 1949, indicating the precipitation back trajectories are representative of the modern climatological mean. Images provided by the NOAA/ESRL Physical Sciences Division, Boulder Colorado (http://www.esrl.noaa.gov/psd/). C) Hydrogen and oxygen isotope results for Indianapolis, IN, precipitation events (gray circles), average $\delta^{18}O$ for the LIA, peak LIA drought between 1400-1450 CE, and minimum LIA $\delta^{18}O$ (blue squares), average $\delta^{18}O$ values for the MCA (orange square), CWP (red square), and modern (green square) $\delta^{18}O$ (orange square). LIA, MCA and CWP $\delta^{18}O_c$ values were converted to VSMOW and then $\delta^{18}O_p$ using the equation Kim and O'Neil (1997) assuming a lake water temperature of 20° C during calcite precipitation. Histograms show the distribution of modern $\delta^{18}O_p$ (blue) and δ^2H_p (red). The solid black line delineates the Regional Meteoric Water Line (RMWL). The dashed black line delineates the Regional Evaporation Line (REL). D) Expanded view of $\delta^{18}O$ and δ^2H values of precipitation (gray circles), regional lakes (blue circles), Martin Lake, IN (green circles), and the MCA, LIA, and CWP (squares indicate $\delta^{18}O_p$ values as described in C). The RMWL-REL intercept (white box) overlaps with the average value of modern Martin Lake waters and the $\delta^{18}O$ of modern calcite. Surface waters from Horseshoe Lake (red circles) plot along the REL.

Figure 2 Plot of the carbon preference index (CPI), average chain length (ACL), and Paq indexes calculated from concentration data. Concentrations of *n*-alkanes C17 through C35 in ug g^{-1} are also shown.

Figure 3 Plot of δ^2H_w results for (A) *n*-C27, (B) *n*-C29, (C) and *n*-C31. Black lines indicate the slopes of each *n*-alkane. (D) Detrended δ^2H_w timeseries for *n*-C31 showing periods of high (red) and low (blue) isotope values relative to the long-term trend.

Figure 4 A) Martin Lake δ^2H results for *n*-C_{27} (green), *n*-C_{29} (red), and *n*-C_{31} (blue). Uncorrected (top) and corrected to δ^2H_p (bottom in parentheses) values are both shown on the y-axis. Solid colored lines represent the different periods of average δ^2H_w values where orange is average, red is elevated, and blues are below average. B) Martin Lake $\delta^{18}O_c$ (black) and $\delta^{13}C_c$ (red) results. C) Lithic abundances (brown) from Martin Lake indicating the frequency and occurrence of warm-season rainstorm events (increasing lithics = increasing warm-season rainstorm events). D) Water table reconstructions from Hole Bog, MN, and Minden Bog, MI. E) δ^2H results from Horseshoe Lake for *n*-C_{24} (green), *n*-C_{26} (red), and *n*-C_{28} (blue). Vertical shaded boxes reflect the Medieval Climate Anomaly (MCA), Little Ice Age (LIA), and current warm period (CWP). Black triangles show the location of ^{14}C ages for the Martin Lake record.

Table 1 Average *δ^2H_p and $\delta^{18}O_c$ during the MCA, LIA, and CWP, and differences between the MCA-LIA and LIA-CWP. Estimated $\delta^{18}O_p$ and expected associated δ^2H_p based on the Martin Lake $\delta^{18}O_c$ values are also shown.

Isotope System	MCA (‰)	LIA (‰)	CWP (‰)	MCA-LIA ‰ Difference	LIA-CWP ‰ Difference
*δ^2H_{C27-p}	-72.7	-64.3	-75.4	-8.4	11.0
*δ^2H_{C29-p}	-68.9	-64.2	-73.8	-4.7	9.6
*δ^2H_{C31-p}	-59.5	-56.5	-69.5	-3.0	13.0
$\delta^{18}O_c$	-9.9	-12.1	-9.5	2.0	-2.6
†$\delta^{18}O_p$	-8.6	-10.8	-8.2	2.2	-2.7
Expected δ^2H_p	-58.8	-76.4	-55.6	17.6	-20.8

*Corrected to VSMOW-Precipitation with epsilon factor of 107 ‰ (Freimuth et al., 2017).
†Converted to $\delta^{18}O_p$ (VSMOW) assuming lake water temperature of 20 ˚C after Kim and O'Neil (1997).

References

Andresen, J., Hilberg, S., Kunkel, K., and Center, M. R. C., 2012, Historical climate and climate trends in the Midwestern USA: US National Climate Assessment Midwest Technical Input Report, p. 1-18.

Baker, R., Gonzalez, L., Raymo, M., Bettis, E., Reagan, M., and Dorale, J., 1998, Comparison of multiple proxy records of Holocene environments in the midwestern United States: Geology, v. 26, no. 12, p. 1131-1134.

Bird, B. W., Barr, R. C., Commerford, J., Gilhooly III, W. P., Wilson, J. J., Finney, B., McLauchlan, K., and Monaghan, G. W., 2019, Late-Holocene floodplain development, land-use, and hydroclimate–flood relationships on the lower Ohio River, US: The Holocene, v. 29, no. 12, p. 1856-1870.

Bird, B. W., Polissar, P. J., Lei, Y., Thompson, L. G., Yao, T., Finney, B. P., Bain, D., Pompeani, D., and Steinman, B. A., 2014, A Tibetan lake sediment record of Holocene Indian summer monsoon variability: Earth and Planetary Science Letters v. 399, p. 92-102.

Bird, B. W., Wilson, J. J., Gilhooly III, W. P., Steinman, B. A., and Stamps, L., 2017, Midcontinental Native American population dynamics and late Holocene hydroclimate extremes: Scientific Reports, v. 7, p. 41628.

Booth, R. K., Notaro, M., Jackson, S. T., and Kutzbach, J. E., 2006, Widespread drought episodes in the western Great Lakes region during the past 2000 years: geographic extent and potential mechanisms: Earth and Planetary Science Letters, v. 242, no. 3, p. 415-427.

Coleman, J. S., and Rogers, J. C., 2003, Ohio River Valley winter moisture conditions associated with the Pacific-North American teleconnection pattern: Journal of climate, v. 16, no. 6, p. 969-981.

Diefendorf, A. F., and Freimuth, E. J., 2017, Extracting the most from terrestrial plant-derived n-alkyl lipids and their carbon isotopes from the sedimentary record: A review: Organic Geochemistry, v. 103, p. 1-21.

Evaristo, J., Jasechko, S., and McDonnell, J. J., 2015, Global separation of plant transpiration from groundwater and streamflow: Nature, v. 525, no. 7567, p. 91-94.

Feakins, S. J., and Sessions, A. L., 2010, Controls on the D/H ratios of plant leaf waxes in an arid ecosystem: Geochimica et Cosmochimica Acta, v. 74, no. 7, p. 2128-2141.

Ficken, K. J., Li, B., Swain, D. L., and Eglinton, G., 2000, An *n*-alkane proxy for the sedimentary input of submerged/floating freshwater aquatic macrophytes: Organic Geochemistry, v. 31, p. 745-749, doi: 710.1016/S0146-6380(1000)00081-00084.

Freimuth, E. J., Diefendorf, A. F., and Lowell, T. V., 2017, Hydrogen isotopes of n-alkanes and n-alkanoic acids as tracers of precipitation in a temperate forest and implications for paleorecords: Geochimica et Cosmochimica Acta, v. 206, p. 166-183.

Freimuth, E. J., Diefendorf, A. F., Lowell, T. V., Bates, B. R., Schartman, A., Bird, B. W., Landis, J. D., and Stewart, A. K., 2020, Contrasting sensitivity of lake sediment n-alkanoic acids and n-alkanes to basin-scale vegetation and regional-scale precipitation δ2H in the Adirondack Mountains, NY (USA): Geochimica et Cosmochimica Acta, v. 268, p. 22-41.

Fricken, K., Li, B., Swain, D. L., and Eglinton, G., 2000, An n-alkane proxy for the sedimentary input of submerged/floating freshwater aquatic macrophytes: Organic Geochemistry, v. 31.7-8, p. 745-749.

Garcin, Y., Schwab, V. F., Gleixner, G., Kahmen, A., Todou, G., Séné, O., Onana, J.-M., Achoundong, G., and Sachse, D., 2012, Hydrogen isotope ratios of lacustrine sedimentary n-alkanes as proxies of tropical African hydrology: insights from a calibration transect across Cameroon: Geochimica et Cosmochimica Acta, v. 79, p. 106-126.

Gat, J. R., 1996, Oxygen and hydrogen isotopes in the hydrologic cycle: Annual Review of Earth and Planetary Sciences, v. 24, p. 255-262.

Gibson, D. K., Bird, B. W., Pollard, H. J., Nealy, C. A., Barr, R. C., and Escobar, J., 2022, Using sediment accumulation rates in floodplain paleochannel lakes to reconstruct climate-flood relationships on the lower Ohio River: Quaternary Science Reviews, v. 298, p. 107852.

Kahmen, A., Hoffmann, B., Schefuß, E., Arndt, S. K., Cernusak, L. A., West, J. B., and Sachse, D., 2013a, Leaf water deuterium enrichment shapes leaf wax n-alkane δD values of angiosperm plants II: Observational evidence and global implications: Geochimica et Cosmochimica Acta, v. 111, p. 50-63.

Kahmen, A., Schefuß, E., and Sachse, D., 2013b, Leaf water deuterium enrichment shapes leaf wax n-alkane δD values of angiosperm plants I: Experimental evidence and mechanistic insights: Geochimica et Cosmochimica Acta, v. 111, p. 39-49.

Kim, S.-T., and O'Neil, J. R., 1997, Equilibrium and nonequilibrium oxygen isotope effects in synthetic carbonates: Geochimica et Cosmochimica Acta v. 61, no. 16, p. 3461-3475.

Laird, K. R., Fritz, S. C., and Cumming, B. F., 1998, A diatom-based reconstruction of drought intensity, duration, and frequency from Moon Lake, North Dakota: a sub-decadal record of the last 2300 years: Journal of Paleolimnology, v. 19, no. 2, p. 161-179.

Leathers, D. J., Yarnel, B., and Plalecki, M. A., 1991, The Pacific/North American teleconnection pattern and the United States climate. Part I: Regional temperature and precipitation associations: Journal of Climate, v. 4, p. 517-528.

Liu, Z., Yoshmura, K., Bowen, G. J., and Welker, J. M., 2014, Pacific–North American teleconnection controls on precipitation isotopes ($\delta^{18}O$) across the contiguous United States and adjacent regions: A GCM-based analysis: Journal of Climate, v. 27, no. 3, p. 1046-1061.

Marzi, R., Torkelson, B., and Olson, R., 1993, A revised carbon preference index: Organic Geochemistry, v. 20, no. 8, p. 1303-1306.

McAndrews, J. H., 1988, Human disturbance of North American forests and grasslands: the fossil pollen record: Vegetation history, p. 673-697.

Munoz, S. E., Gruley, K. E., Massie, A., Fike, D. A., Schroeder, S., and Williams, J. W., 2015, Cahokia's emergence and decline coincided with shifts of flood frequency on the Mississippi River: Proceedings of the National Academy of Sciences, v. 112, no. 20, p. 6319-6324.

Muñoz, S. E., Porter, T. J., Bakkelund, A., Nusbaumer, J., Dee, S. G., Hamilton, B., Giosan, L., and Tierney, J. E., 2020, Lipid biomarker record documents hydroclimatic variability of the Mississippi River basin during the Common Era: Geophysical Research Letters, v. 47, no. 12, p. e2020GL087237.

Munoz, S. E., Schroeder, S., Fike, D. A., and Williams, J. W., 2014, A record of sustained prehistoric and historic land use from the Cahokia region, Illinois, USA: Geology, v. 42, no. 6, p. 499-502.

New, J. F., 2009, Oliver, Olin, and Martin Lakes diagnostic study La Grange County, Indiana.

Pompeani, D., Bird, B. W., Wilson, J. J., Abbott, M. B., Finkenbinder, M. S., and Hillman, A. L., 2021, Severe Little Ice Age drought in the midcontinental United States during the Mississippian abandonment of Cahokia: Scientific Reports, v. 11, no. 1, p. 1-8.

Puleo, P. J., Axford, Y., McFarlin, J. M., Curry, B. B., Barklage, M., and Osburn, M. R., 2020, Late glacial and Holocene paleoenvironments in the midcontinent United States, inferred from Geneva Lake leaf wax, ostracode valve, and bulk sediment chemistry: Quaternary Science Reviews, v. 241, p. 106384.

Rao, Z., Zhu, Z., Jia, G., Henderson, A. C., Xue, Q., and Wang, S., 2009, Compound specific δD values of long chain n-alkanes derived from terrestrial higher plants are indicative of the δD of meteoric waters: Evidence from surface soils in eastern China: Organic Geochemistry, v. 40, no. 8, p. 922-930.

Sachse, D., Billault, I., Bowen, G. J., Chikaraishi, Y., Dawson, T. E., Feakins, S. J., Freeman, K. H., Magill, C. R., McInerney, F. A., and Van Der Meer, M. T., 2012, Molecular paleohydrology: interpreting the hydrogen-isotopic composition of lipid biomarkers from photosynthesizing organisms: Annual Review of Earth and Planetary Sciences, v. 40, p. 221-249.

Sachse, D., Radke, J., and Gleixner, G., 2004, Hydrogen isotope ratios of recent lacustrine sedimentary n-alkanes record modern climate variability: Geochimica et Cosmochimica Acta, v. 68, no. 23, p. 4877-4889.

Schartman, A. K., Diefendorf, A. F., Lowell, T. V., Freimuth, E. J., Stewart, A. K., Landis, J. D., and Bates, B. R., 2020, Stable source of Holocene spring precipitation recorded in leaf wax hydrogen-isotope ratios from two New York lakes: Quaternary Science Reviews, v. 240, p. 106357.

Smith, F. A., and Freeman, K. H., 2006, Influence of physiology and climate on δD of leaf wax n-alkanes from C3 and C4 grasses: Geochimica et Cosmochimica Acta, v. 70, no. 5, p. 1172-1187.

Suh, Y. J., Diefendorf, A. F., Bowen, G. J., Cotton, J. M., and Ju, S.-J., 2019, Plant wax integration and transport from the Mississippi River Basin to the Gulf of Mexico inferred from GIS-enabled isoscapes and mixing models: Geochimica et Cosmochimica Acta, v. 257, p. 131-149.

Thomas, E. K., Clemens, S. C., Prell, W. L., Herbert, T. D., Huang, Y., Liu, Z., Sinninghe Damsté, J. S., Sun, Y., and Wen, X., 2014, Temperature and leaf wax δ2H records demonstrate seasonal and regional controls on Asian monsoon proxies: Geology, v. 42, no. 12, p. 1075-1078.

Tierney, J. E., Russell, J. M., Huang, Y., Damsté, J. S. S., Hopmans, E. C., and Cohen, A. S., 2008, Northern hemisphere controls on tropical southeast African climate during the past 60,000 years: Science, v. 322, no. 5899, p. 252-255.

Tipple, B. J., Berke, M. A., Doman, C. E., Khachaturyan, S., and Ehleringer, J. R., 2013, Leaf-wax n-alkanes record the plant–water environment at leaf flush: Proceedings of the National Academy of Sciences, v. 110, no. 7, p. 2659-2664.

Webb, T., 1985, Holocene palynology and climate: Paleoclimate Analysis and Modeling. Wiley-Interscience, New York, p. 163.

Williams, A. S., 1974, Late-glacial-postglacial vegetational history of the Pretty Lake region, northeastern Indiana: US Govt. Print. Off., 2330-7102.

Wright, M. N., Bird, B. W., Gibson, D. K., Pollard, H., Escobar, J., and Barr, R. C., 2023, Fluvial responses to late Holocene hydroclimate variability in the midcontinental United States: Quaternary Science Reviews, v. 301, p. 107939.

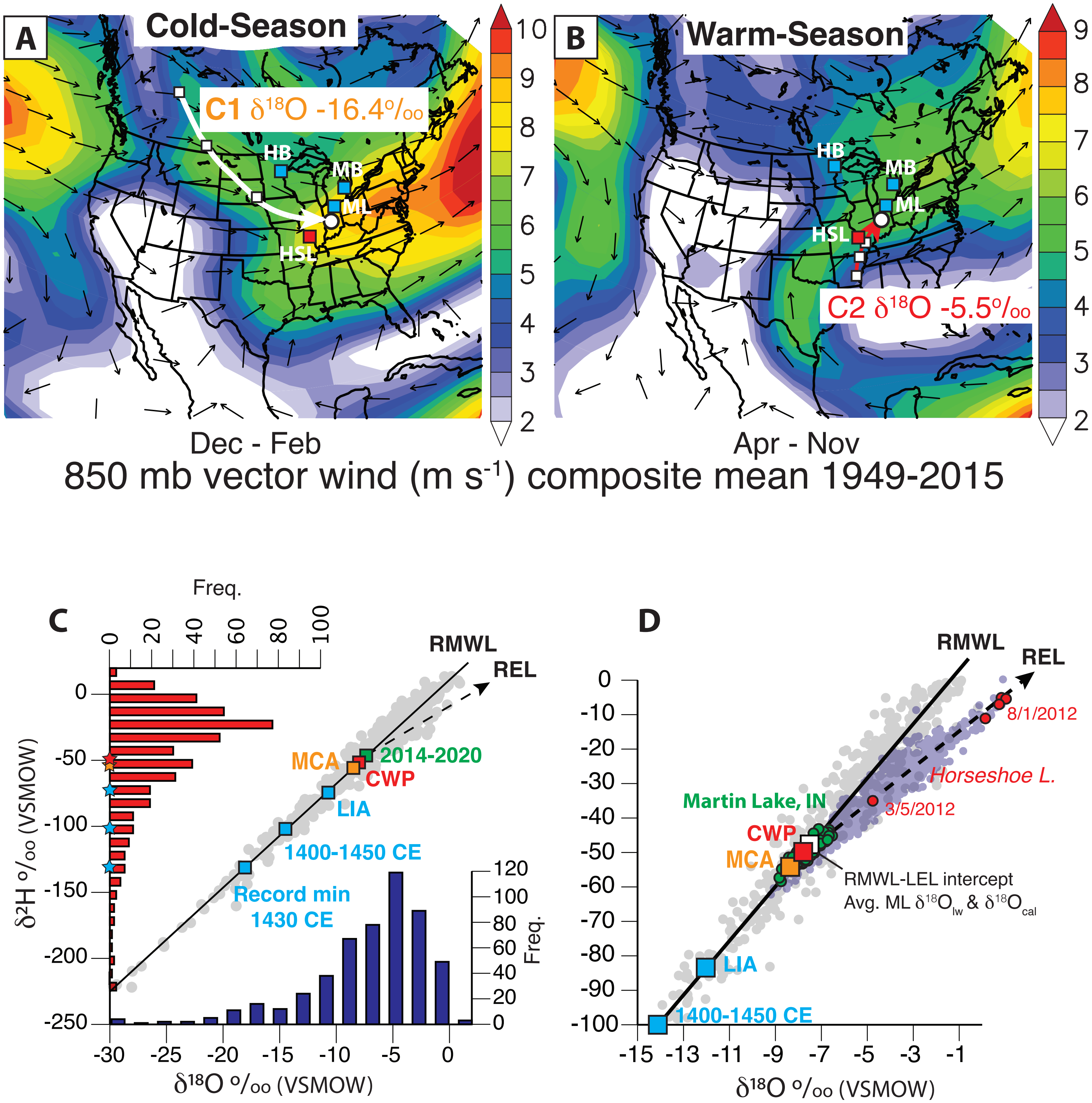
A
Cold-Season
C1 δ18O -16.4‰
HB
MB
ML
HSL
10
9
8
7
6
5
4
3
2
Dec - Feb
B
Warm-Season
HB
MB
ML
HSL
C2 δ18O -5.5‰
9
8
7
6
5
4
3
2
Apr - Nov
850 mb vector wind (m s-1) composite mean 1949-2015
C
Freq.
0
20
40
60
80
100
RMWL
REL
MCA
2014-2020
CWP
LIA
1400-1450 CE
Record min
1430 CE
120
100
80
60
40
20
0
Freq.
0
-50
-100
-150
-200
-250
δ2H ‰ (VSMOW)
-30
-25
-20
-15
-10
-5
0
δ18O ‰ (VSMOW)
D
RMWL
REL
0
-10
-20
-30
-40
-50
-60
-70
-80
-90
-100
8/1/2012
Horseshoe L.
3/5/2012
Martin Lake, IN
CWP
MCA
RMWL-LEL intercept
Avg. ML δ18Olw & δ18Ocal
LIA
1400-1450 CE
-15
-13
-11
-9
-7
-5
-3
-1
δ18O ‰ (VSMOW)

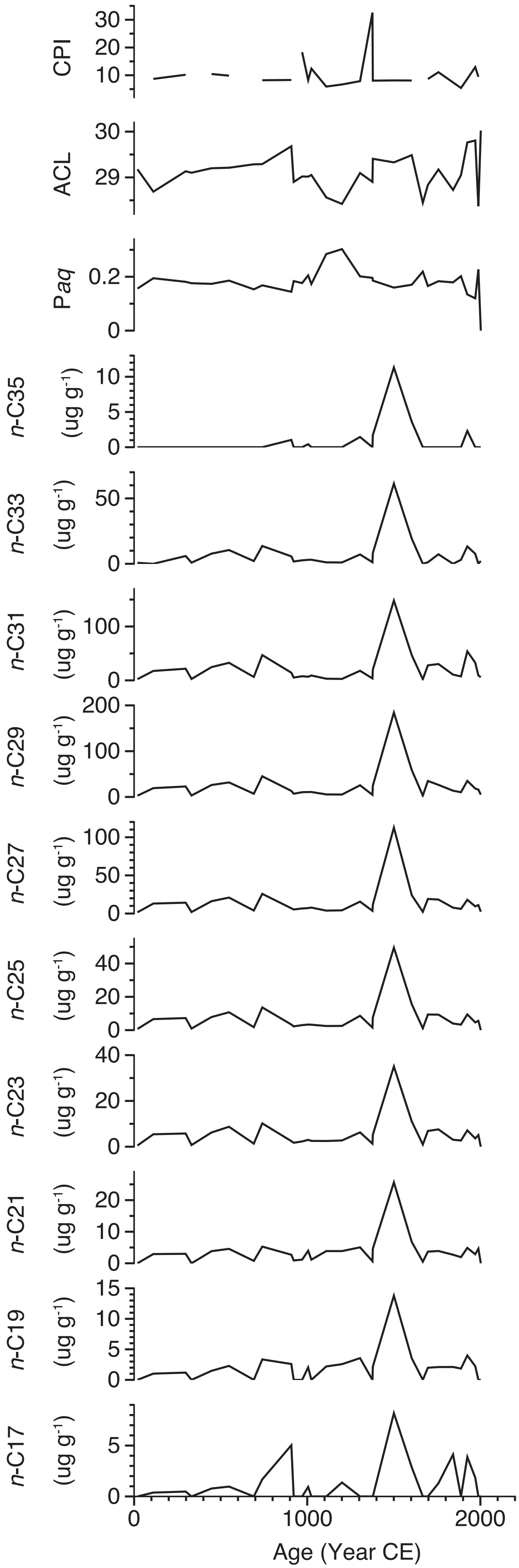
CPI
ACL
Paq
n-C35 (ug g-1)
n-C33 (ug g-1)
n-C31 (ug g-1)
n-C29 (ug g-1)
n-C27 (ug g-1)
n-C25 (ug g-1)
n-C23 (ug g-1)
n-C21 (ug g-1)
n-C19 (ug g-1)
n-C17 (ug g-1)
Age (Year CE)

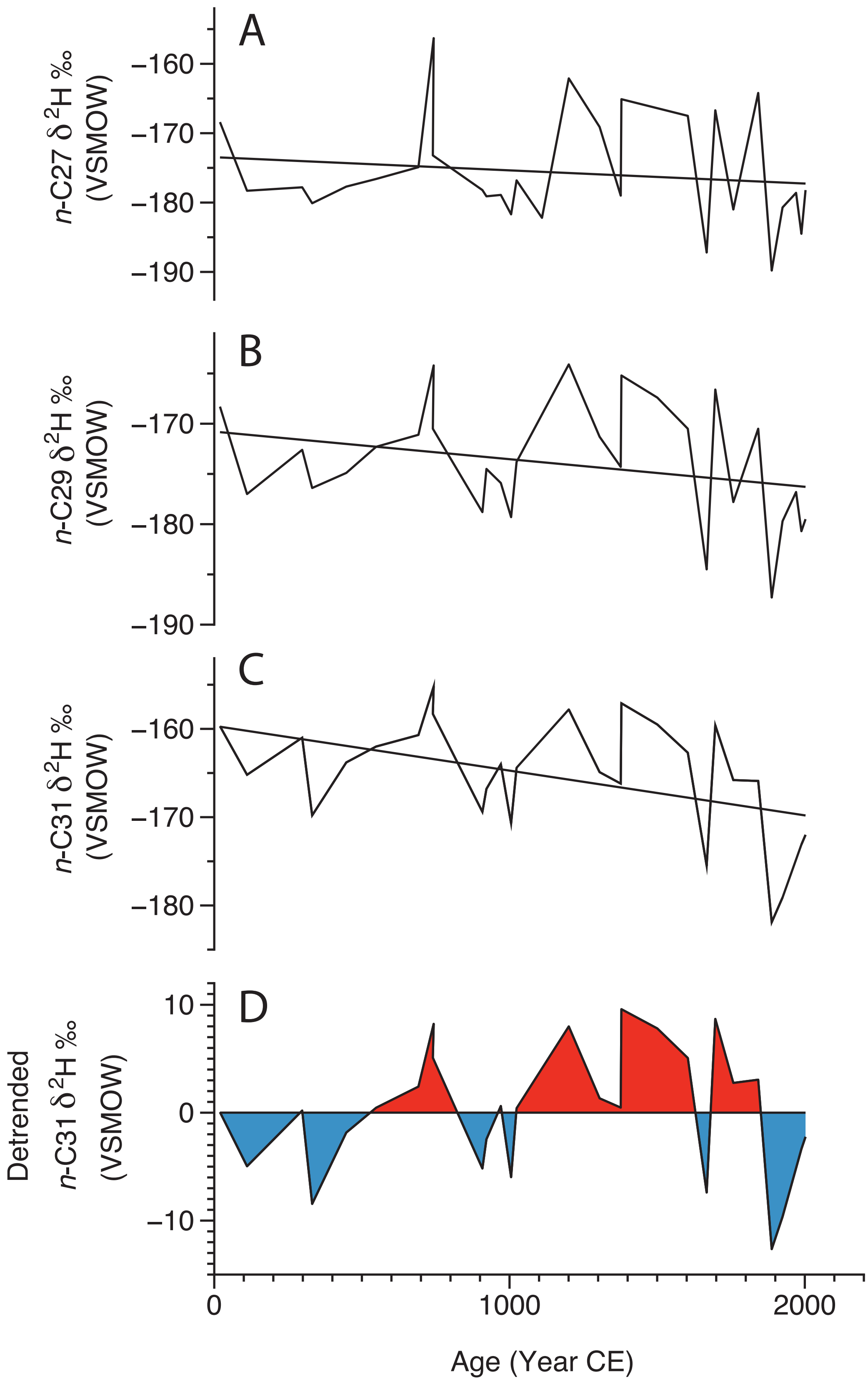

A
B
C
D
n-C27 δ2H ‰ (VSMOW)
n-C29 δ2H ‰ (VSMOW)
n-C31 δ2H ‰ (VSMOW)
Detrended n-C31 δ2H ‰ (VSMOW)
−160
−170
−180
−190
−170
−180
−190
−160
−170
−180
10
0
−10
0
1000
2000
Age (Year CE)

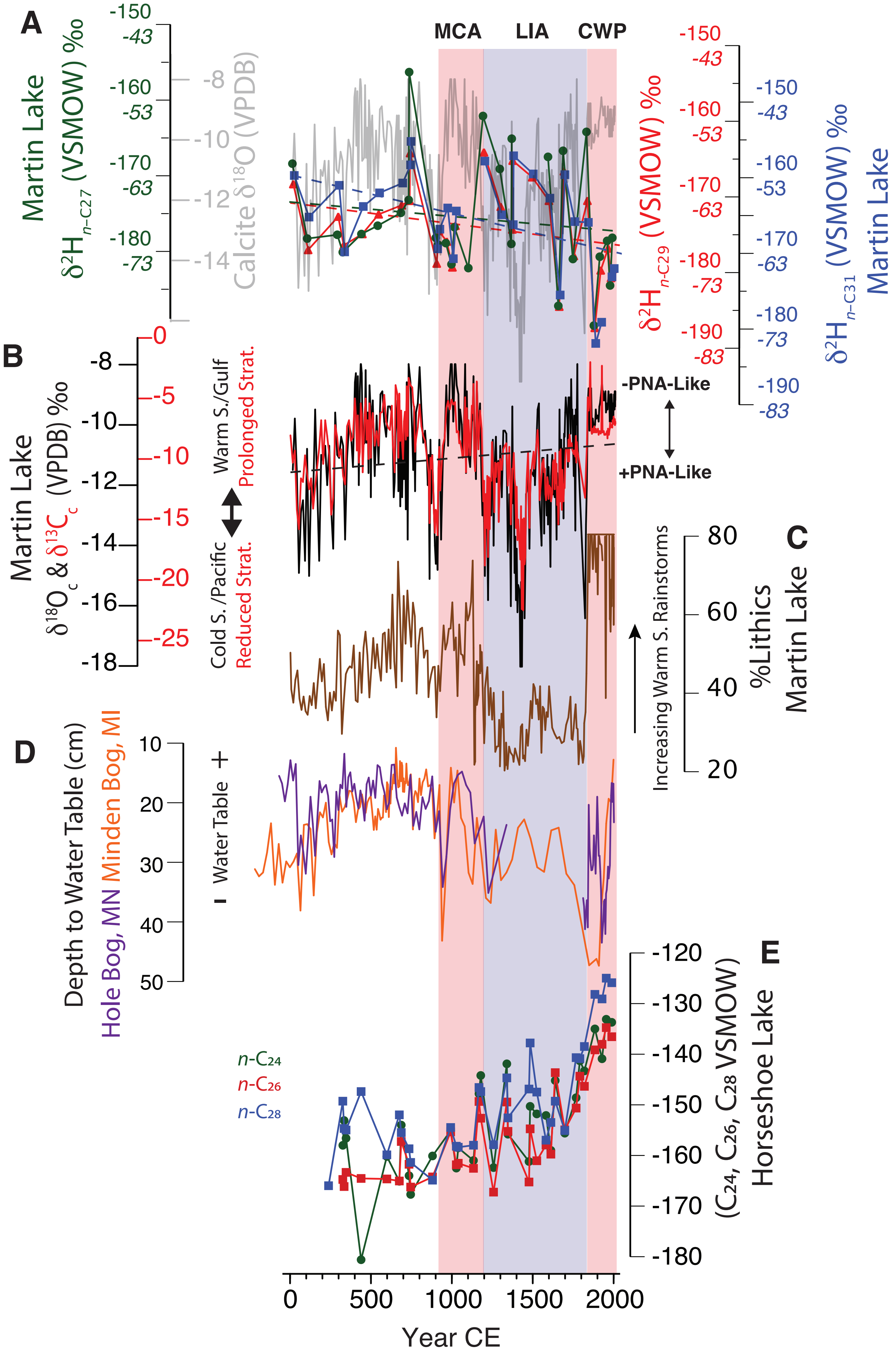
A
B
C
D
E
MCA
LIA
CWP
Martin Lake
δ2Hn-C27 (VSMOW) ‰
Calcite δ18O (VPDB)
δ2Hn-C29 (VSMOW) ‰
δ2Hn-C31 (VSMOW) ‰
Martin Lake
δ18Oc & δ13Cc (VPDB) ‰
Warm S./Gulf
Prolonged Strat.
Cold S./Pacific
Reduced Strat.
-PNA-Like
+PNA-Like
Increasing Warm S. Rainstorms
%Lithics
Martin Lake
Depth to Water Table (cm)
Hole Bog, MN Minden Bog, MI
+ Water Table -
n-C24
n-C26
n-C28
(C24, C26, C28 VSMOW)
Horseshoe Lake
Year CE